

# Chapter 5

## Application of High-Frequency Damage Detection Methods to Benchmark Problems

To validate the high-frequency damage detection methods developed in previous chapters, the methods were applied to two damage-detection datasets, including a small-scale nonlinear frame made available by the Los Alamos National Laboratory (LANL) and a damaged cable-stayed bridge in China that was made available by the Center of Structural Monitoring and Control at the Harbin Institute of Technology.

### 5.1 Nonlinear Frame

Nonlinear damage was experimentally studied in a three-story frame with an installed bumper mechanism (Figueiredo and Flynn, 2009). The three-story frame structure (0.6 m tall), shown in Figure 5.1, consists of aluminum columns and plates connected by bolted joints. A shaker excites the base of the structure along a single axis with white noise with an excitation bandwidth of 20-150 Hz. The structure is instrumented with four accelerometers, one at each floor and the base. A sampling frequency of 320 Hz, is used for a duration of 25.6 seconds. The force at the base of the structure applied by the shaker is also recorded.

‘Damage’ is introduced by a bumper mechanism that creates a repetitive, impact-type nonlinearity. According to Figueiredo and Flynn (2009), the mechanism is intended to

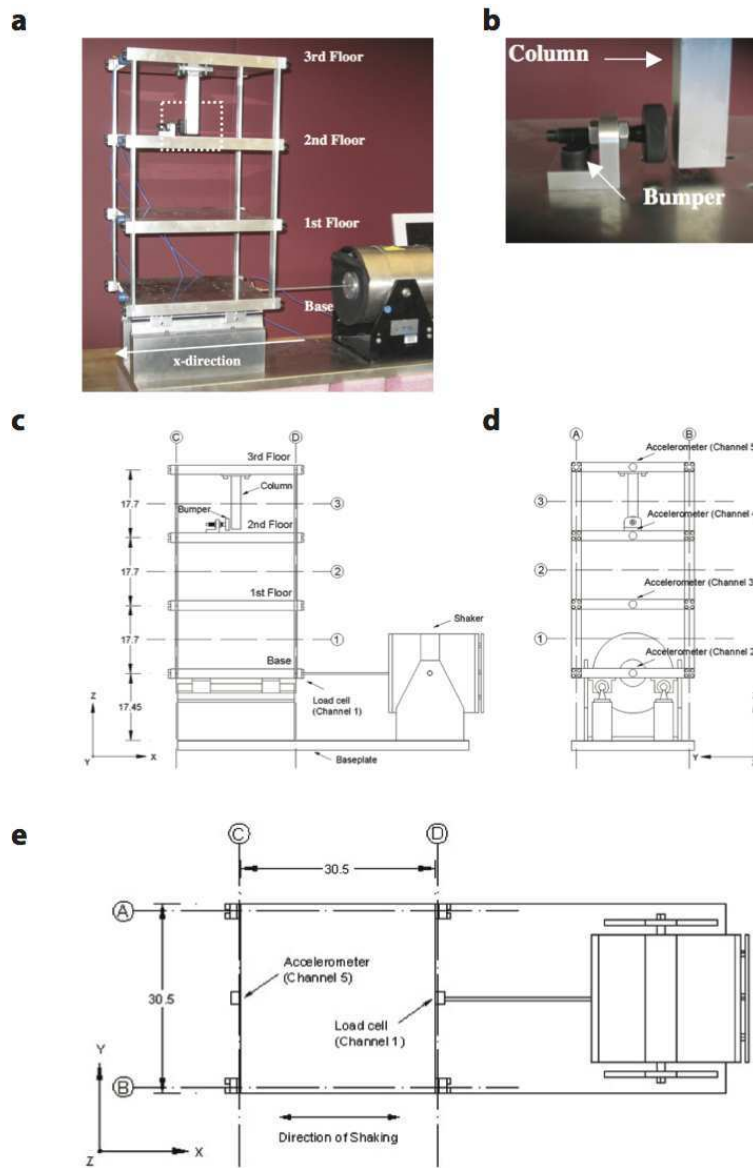


Figure 5.1: **LANL Nonlinear Frame: Experimental Setup.** **a**, The three-story frame structure (0.6 m tall) consists of aluminum columns and plates connected by bolted joints. **b**, ‘Damage’ is introduced by a bumper mechanism that creates a repetitive, impact-type nonlinearity. The bumper device is installed between the 2nd and 3rd floors, and consists of a bumper device on the second floor that is able to collide with a center column that extrudes from the base of the top floor. The level of damage is varied by adjusting the distance between the bumper and the column when the structure is in a resting position. **c**, A shaker excites the base of the structure along a single axis with white noise with an excitation bandwidth of 20-150 Hz. **d**, The structure is instrumented with four accelerometers, one at each floor and the base. A sampling frequency of 320 Hz, is used for a duration of 25.6 seconds. **e**, The force at the base of the structure applied by the shaker is also recorded. Images courtesy of Figueiredo and Flynn (2009).

simulate nonlinearities created by damage, such as a crack that opens and closes under dynamic loads (known as a ‘breathing crack), or loose connections that rattle. The bumper mechanism is installed between the second and third floors, and consists of a bumper on the second floor that is able to collide with a center column that extrudes from the base of the top floor. The level of damage is varied by adjusting the distance between the bumper and the column when the structure is in a resting position.

The following levels of damage are studied in this section:

**Undamaged**          Baseline condition

**Damage Level 1**    Gap (0.20 mm)

**Damage Level 2**    Gap (0.15 mm)

**Damage Level 3**    Gap (0.13 mm)

**Damage Level 4**    Gap (0.10 mm)

**Damage Level 5**    Gap (0.05 mm)

Studies on this data set that have previously been published are mentioned here. Karaiskos et al. (2012) applied outlier methods to modal filtering methods and auto-regressive parameters to detect damage. Hernandez-Garcia et al. (2010) used a MDOF lumped-mass model with additional nonlinear elements to model the behavior of the frame. A correlation was found between the length of the gap created and the magnitude of the observed changes in the nonlinear coefficients (i.e., restoring force coefficients). Figueiredo et al. (2011) applied a few different machine learning algorithms, including neural network, factor analysis, Mahalanobis distance, and singular value decomposition. Bornn et al. (2010) applied an auto-regressive support vector machine algorithm with outlier analysis. Figueiredo et al. (2009) combined support vector machines with outlier analysis to identify and localize damage between the top two stories.

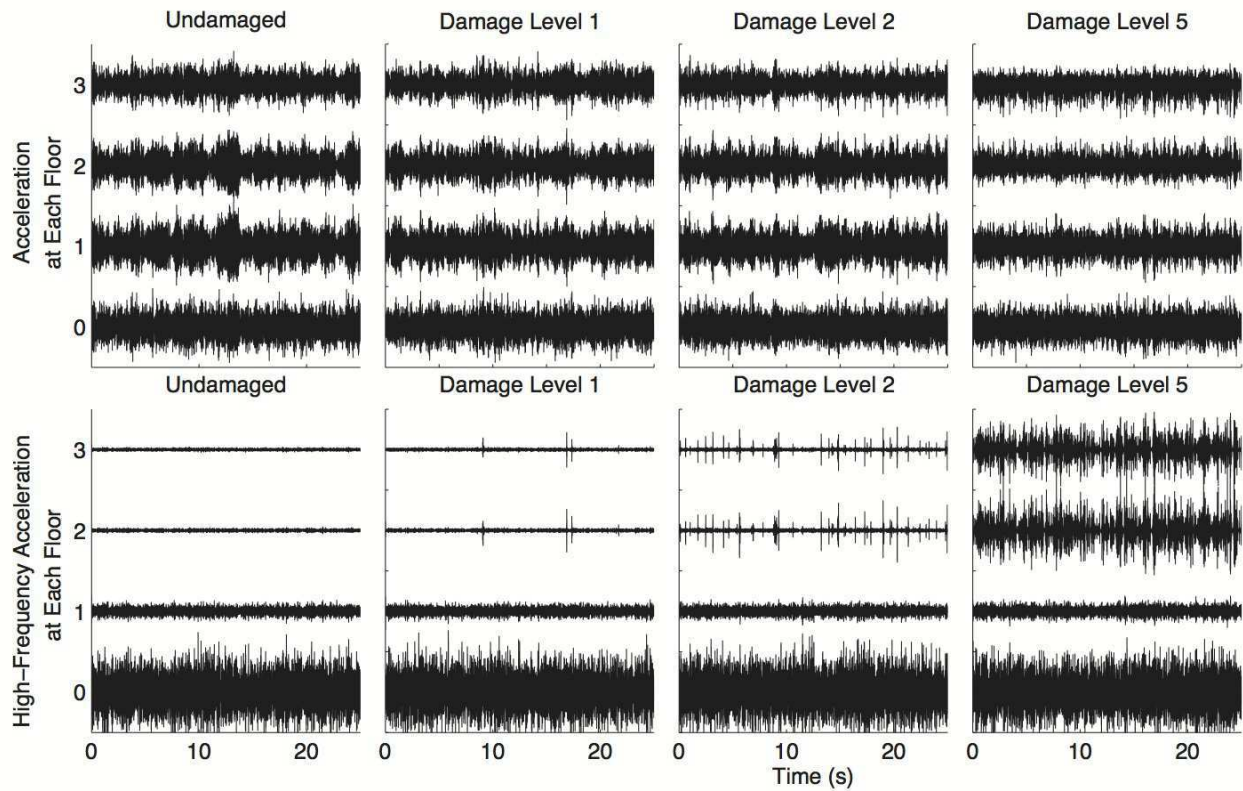


Figure 5.2: **LANL Nonlinear Frame: Recorded Accelerations (Raw and High-Pass Filtered).** By high-pass filtering ( $8^{th}$  order Butterworth filter with a cut-off frequency of 88 Hz) the data, the bumper impact events are clearly identified as high-frequency short-duration pulses. The increase in damage results in an increase in the number of impacts. While the impact events are clearly separated in time during Damage Levels 1 and 2, it becomes difficult to distinguish between different damage events for Damage Level 5.

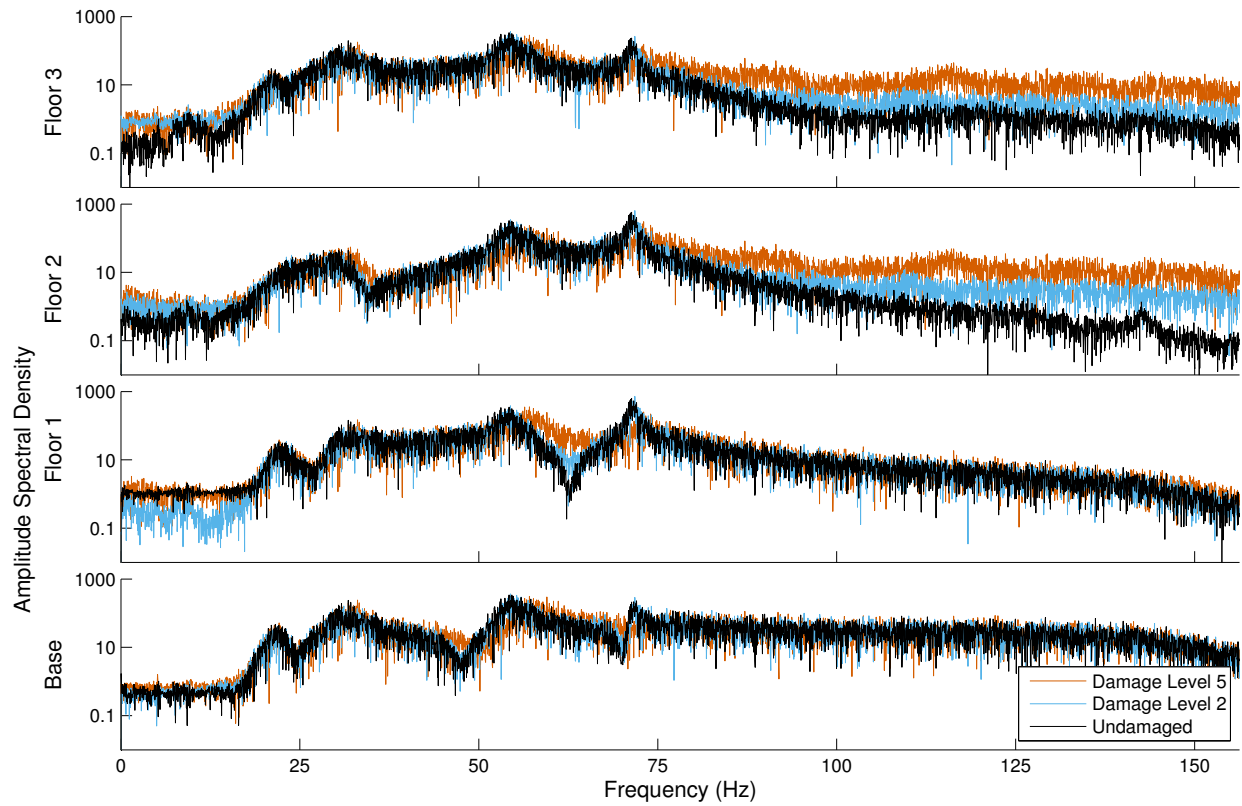


Figure 5.3: **LANL Nonlinear Frame: Amplitude Spectral Density.** The amplitude spectral densities are calculated from the magnitude of the Fourier transform of the raw accelerations. The amplitude spectral densities capture the increase in high-frequency energy that is generated during the bumper impacts between Floors 2 and 3. It appears that there is a significant amount of energy in the system above 160 Hz, and a higher sampling rate could have been used.

### 5.1.1 Identification of Damage Signals Through Feature Extraction of Pulses

The response of the structure to the impact of the bumper device can be clearly distinguished from the predominant modal response (the first three modes) of the structure by applying a high-pass filter. As the natural frequencies of the first three modes are approximately 30 Hz, 55 Hz, and 70 Hz, an 8<sup>th</sup> order Butterworth filter with a cut-off frequency of 88 Hz is chosen. Pulses in the resulting high-frequency accelerations, shown in Figure 5.2, capture the motion of elastic waves that are generated by the impact of the column with the bumper. The amplitude and frequency content of these signals make them clearly observable over the predominant modal response, and their relatively sparse occurrence at lower levels of damage make them easy to identify and track. On the other hand, at Damage Level 5, impacts occur so frequently that it becomes difficult to distinguish between individual events. In fact, the high-frequency acceleration recorded on Floors 2 and 3 for Damage Level 5 begins to resemble that recorded at the base of the structure. The motion at the base created by the shaker most likely consists of many tiny stick-slip events, with each event exciting elastic waves that propagate within the base floor. This is presumably what causes the much higher frequency content observed in the base floor (and, arguably, the first floor by proximity). This results in a low signal-to-noise ratio recorded on the first and base floor, making it difficult to detect the propagation of the elastic wave generated from the bumper impacts to the first floor or base in the time-domain. In analyzing the frequency content recorded on each floor for three different damage levels, shown in Figure 5.3, the amplitude spectral densities remain relatively constant between the undamaged and damaged cases. A clear increase in the amplitude spectral density occurs above 75 Hz on Floors 2 and 3, for increasing levels of damage. Hence, it appears that the high-frequency energy generated by the impact of the bumper with the column does not propagate to the first floor.

By using a time-frequency representation of the Floor 3 acceleration records, shown in Figure 5.4, occurrences of the high-frequency impact events clearly stand out from the modal response. A comparison of the spectrograms generated for each floor in Damage Level 2

further confirms that the damage signal is confined to the top two floors. The spectrograms were generated by partitioning the signal in time (a time-window length of 128 points), applying a Hamming window, taking the Fourier Transform, and plotting the logarithm of the power spectral density of each segment. In Figure 5.4, the occurrences of impacts are manifested as vertical stripes, occurring during a very short time span over a burst of frequencies. The events are clearly distinguished from one another at lower levels of damage. At Damage Level 5, the spectrogram begins to resemble white noise at higher frequencies. From Figure 5.5, the bumper impacts are clearly evident on Floors 2 and 3, but not on Floor 1 or the Base. Hence, damage is localized to Floors 2, 3, or both. Additional analysis methods would be needed to localize the source of damage to a more precise location within the top two floors. As hammer-blow data is not available and the low sampling rate does not make for a precise determination of arrival time, forward modeling (i.e., a highly-discretized numerical model) would be needed to estimate the relative amplitudes in acceleration that would occur in response to damage introduced at different locations within Floors 2 and 3.

Following the method described in Section 3.3.4, templates are constructed from the high-frequency impulses that are detected first, namely those in the Damage Level 1 acceleration time series. Shown in Figure 5.6, the high-frequency signals generated by the bumper impacts are not well-characterized at a sampling rate of 320 Hz. The original signals appear to contain a significant amount of energy at higher frequencies. It might be possible to recover some of this information using signal processing techniques, but for now we will use these two templates to try to detect repeating events in subsequent trials. It is worth noting that in an actual building, one might encounter similar technical issues (i.e., decimation and possibly subsampling of a signal generated by damage), and it is better to test the performance of the method for small-scale structures under suboptimal conditions before applying the method to buildings with similar technical limitations.

The high-frequency signals recorded on Floors 2 and 3 are similar to one another in waveform and amplitude, but the polarity is reversed. This can be explained by the force mechanisms of the bumper device. When an impact occurs, an equal and opposite force is generated on each side of the device at the moment of impact, and hence an equal and

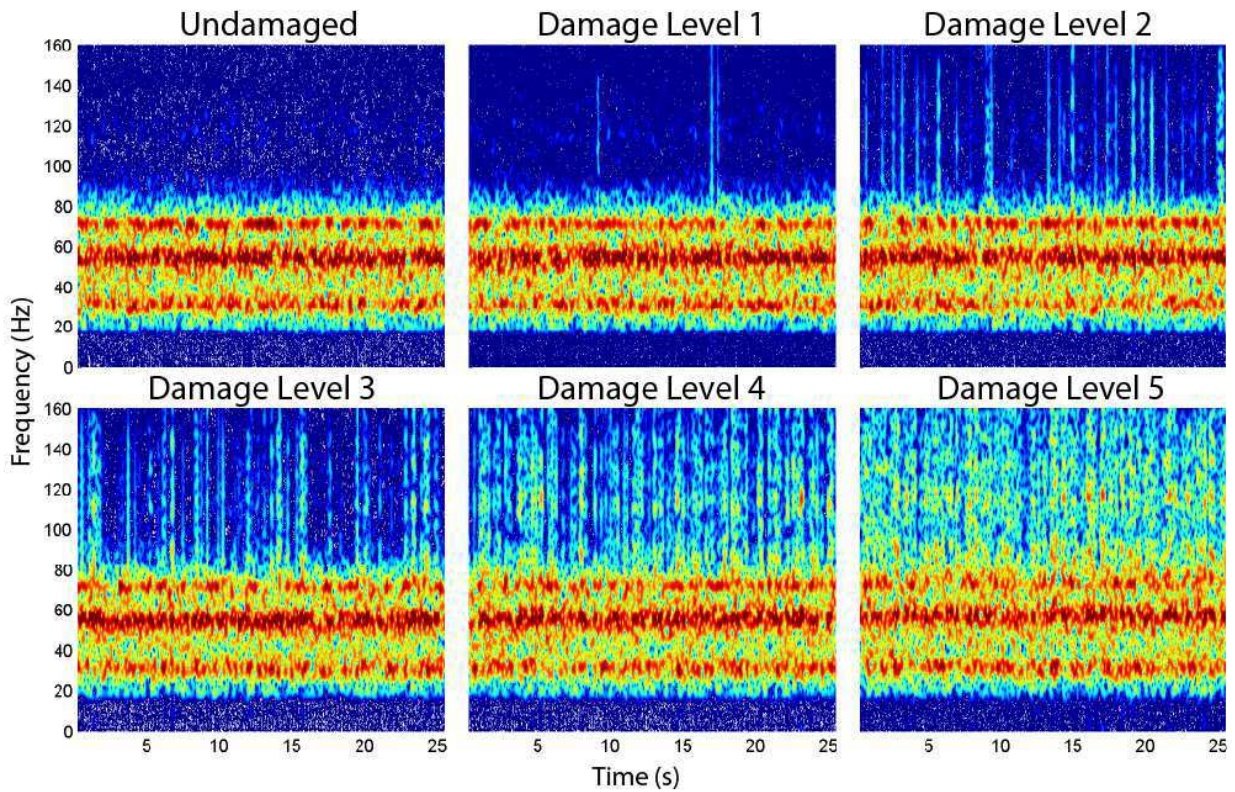


Figure 5.4: **LANL Nonlinear Frame: Spectrograms for Different Damage Levels.** Occurrences of the high-frequency impact events clearly stand out from the modal response and are manifested as vertical stripes, occurring during a very short time span over a burst of frequencies.

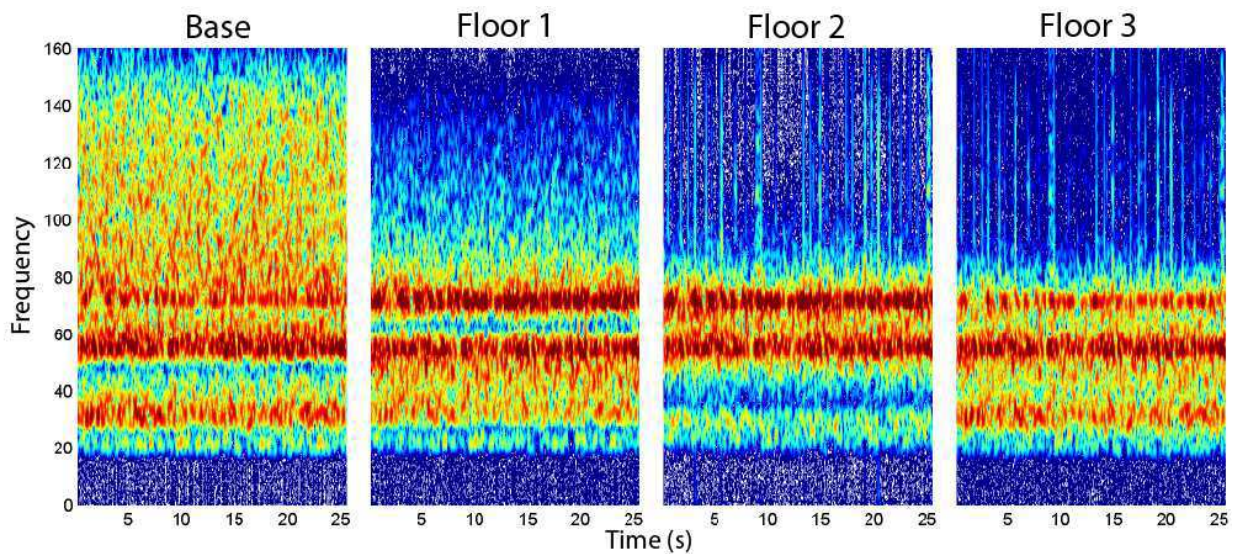


Figure 5.5: **LANL Nonlinear Frame: Spectrograms for Different Floors at Damage Level 2.** Damage events are clearly observed on Floors 2 and 3.

opposite force is applied to Floors 2 and 3. Only the accelerations recorded at the stations on Floors 2 and 3, with a high signal-to-noise-ratio of the detected high-frequency signal, are used to create the templates. For this reason, a high threshold value of 0.9 is chosen, though lower values are observed to work as well. The templates are cross-correlated with the acceleration recorded for Damage Levels 2-5, and detection of repeating signals (i.e., a cross-correlation value above the threshold) is highlighted in Figure 5.7. Despite the issues with the sampling rate, the method still works well, though an increase in false negatives is observed. Template 1 (the blue signal) is detected many more times than Template 2 (the orange signal), as Template 2 appears to consist of two separate events. The total number of detected occurrences of the repeating signals in each record is as follows: Undamaged: 0, Damage Level 1: 3, Damage Level 2: 17, Damage Level 3: 51, Damage Level 4: 49, Damage Level 5: 38. Clearly, there are a number of false negatives in the Damage Level 4 and 5 acceleration records, made evident by the undetected pulses. This reduction in performance seems to be related to the frequent occurrence of pulses, many of which are not well-separated in time. The number of false negatives could be improved on by using a shorter template that has fewer zero-values, using a lower threshold value, or updating the templates.

Finally, in addition to increasing the sampling rate, one potential improvement to this study would be to equip the bumper-column device with an open circuit that closes whenever the bumper and column come into contact. It would then be possible to record exactly when the damage events occurs, and the number of false positives and negatives could be confidently compared to those obtained from the high-frequency analysis.

## 5.2 Damaged Cable-Stayed Bridge in China

Data recorded on a damaged cable-stayed bridge in China was made available by the Center of Structural Monitoring and Control at the Harbin Institute of Technology. First opened to traffic in 1987, the bridge is one of the first built cable-stayed bridges in mainland China. According to Li et al. (2013), the bridge was repaired between 2005 and 2007 for cracks observed at the bottom of a girder segment over the mid-span, and corroded stay cables

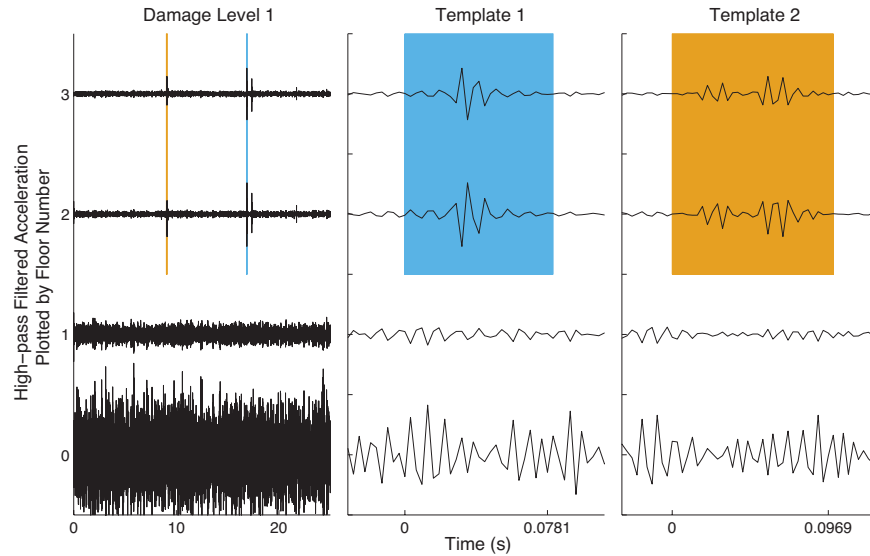


Figure 5.6: **LANL Nonlinear Frame: Damage Signals.** Damage signals are clearly identified in the acceleration records as high-frequency short-duration pulses.

(especially those near the anchors). During this time, the bridge was also upgraded with an SHM system that includes more than 150 sensors, including 14 uniaxial accelerometers, 1 biaxial accelerometer, an anemoscope, a temperature sensor, and optical fiber Bragg grating sensors. Li et al. (2013) presume that the bridge was damaged gradually over a time period from January to August 2008 by overloading.

Acceleration data were recorded continuously by 14 uniaxial accelerometers permanently installed on the deck and 1 biaxial accelerometer fixed to the top of one of the towers to monitor the tower's horizontal acceleration. The dimensions of the bridge as well as the instrument layout are shown in Figure 5.10. Data were recorded between January and August, during which time the bridge transitioned from being in an undamaged state to being in a damaged state. A full day of acceleration data recorded at 100 sps is made available approximately twice a month during this time period. The benchmark problem is to detect, localize, and quantify damage using acceleration measured during this time period. The specific dates are: January 1, January 17, February 3, March 19, March 30, April 9, May 5, May 18, May 31, June 7, June 16, and July 31, 2008.

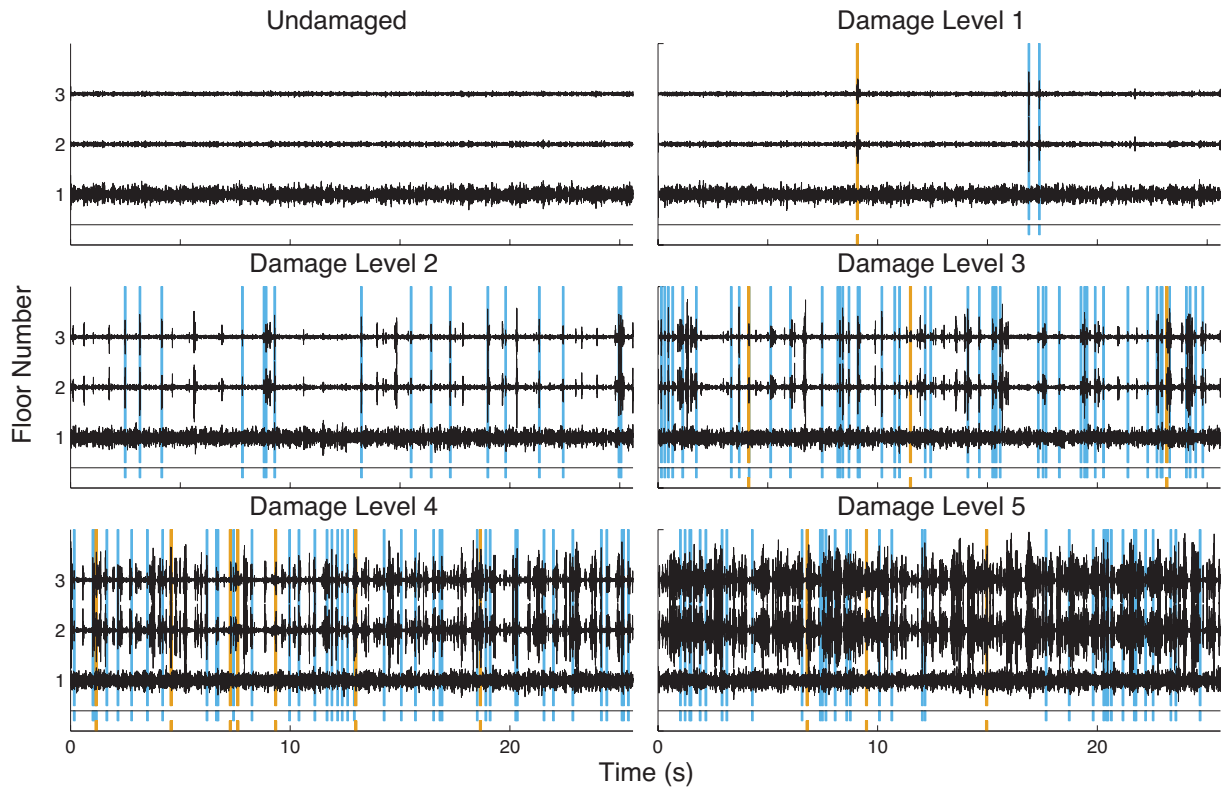


Figure 5.7: **LANL Nonlinear Frame: Damage Detection.** The two damage signals identified in the Damage Level 1 acceleration data are used as templates to detect damage in subsequent records. Only the top two floors are used in the subsequent analysis, with a threshold value of 0.9. A running cross-correlation is performed with auto-correlation normalization, and when the stacked correlation value exceeds the threshold, the signal is said to have been detected. The total number of detected occurrences of the repeating signals in each record is as follows: Undamaged: 0, Damage Level 1: 3, Damage Level 2: 17, Damage Level 3: 51, Damage Level 4: 49, Damage Level 5: 38.

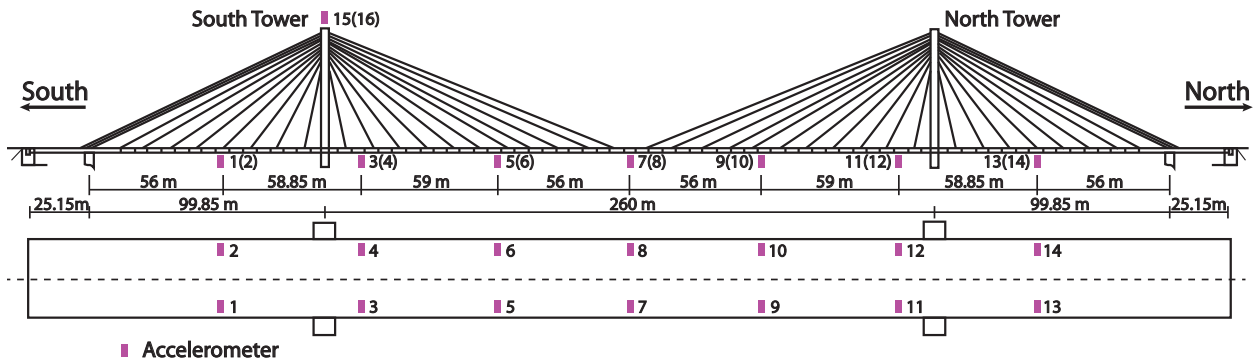


Figure 5.8: **Cable-Stayed Bridge: Dimensions and Instrument Layout.** One of the earliest cable-stayed bridges constructed in mainland China, the bridge consists of a main span of 260m and two side spans of 25.15+99.85 m each. The bridge was upgraded with an SHM system that includes more than 150 sensors, including 14 uniaxial accelerometers, 1 biaxial accelerometer, an anemoscope, a temperature sensor, and optical fiber Bragg grating sensors. This figure was adapted from a similar figure in Li et al. (2013).

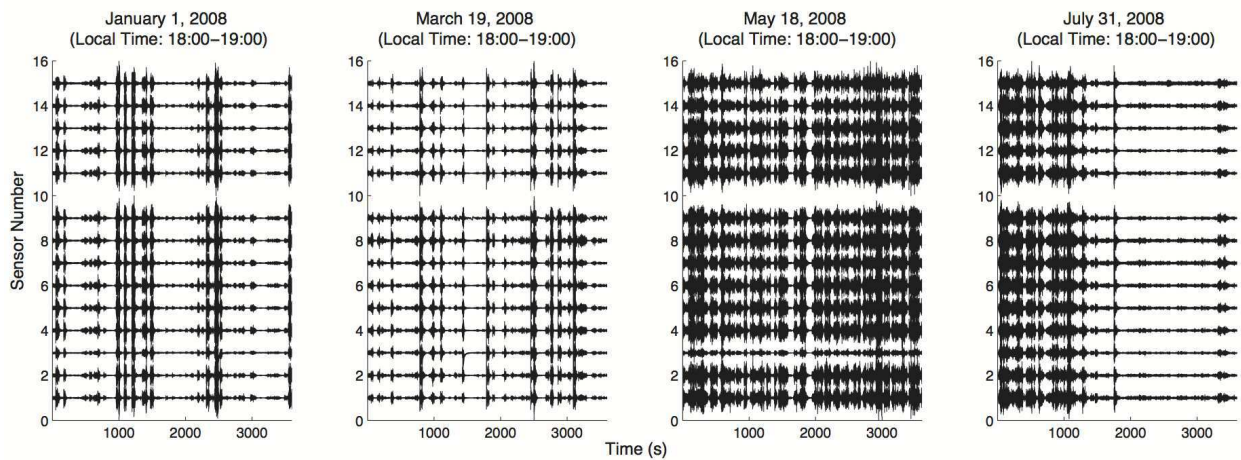


Figure 5.9: **Cable-Stayed Bridge: Sample Deck Accelerations.** Sample accelerations recorded by the accelerometers installed on the deck are shown during seven months when the bridge progressed from being in an undamaged state (in January) to being in a damaged state (in July). An increase in high-frequency short-duration pulses is clearly observed in the acceleration records. The occurrence of these pulses alone might be used to indicate the presence of damage. The abrupt decrease in acceleration levels around 18:30 on July 31 was caused by preventative measures that were taken to limit traffic to prevent the collapse of the bridge (Li et al., 2013). This indicates that the pulses are primarily caused by traffic. The data were high-pass filtered using a 2<sup>nd</sup> order Butterworth filter with a cut-off frequency of 5 Hz.

## 5.2.1 Identification of Damage Signals Through Feature Extraction of Pulses

Sample acceleration records from January 1, March 19, March 18, and July 31 during times of heavy traffic are shown in Figure 5.9. The May 18 record is representative of the acceleration time series during the same time of day on June 7 and June 16. The January 1 and March 19 records are representative of records before May 18. The abrupt decrease in acceleration levels around 18:30 on July 31 was caused by preventative measures that were taken to limit traffic to prevent the collapse of the bridge (Li et al., 2013). It is concluded that the presence of damage results in the increased presence of high-frequency short-duration pulses that are primarily generated by vehicle traffic. Indeed, Li et al. (2013) similarly observe that higher magnitude accelerations were observed in the damage state, as well as a significant change in the power spectral density.

By analyzing the acceleration records (Figures 5.11 5.12 5.13, and 5.14) during a time interval (local time of 00:00-01:00) when light traffic is expected on the bridge, an increase in the occurrence of high-frequency short-duration signals with the presence of damage is also observed to have occurred, and fewer pulses are excited during light traffic than are excited during heavy traffic. The pulse events have clear separation in time and appear to be repeating in nature. The feature extraction method is followed. First, a pulse is identified in the undamaged state,  $T_1^{UD}$  (yellow), and is shown in Figure 5.10. The undamage signal is a horizontally-propagating wave that has large vertical component, a duration shorter than 1 s, and an apparent velocity of greater than 300 m/s (671 miles per hour). The signal originates at the north end of the bridge, and could be due to the dynamic response of the bridge to the rapid loading generated as a vehicle drives onto or off the bridge, possibly over a location that has increased flexibility. It might be possible to use a simple finite-element model combined with information about the bridge, such as the speed limit and average vehicle load, to determine which mechanism generates the pulse.

The undamage signal is detected multiple times in each subsequent record recorded at the same local time. A threshold value of 0.35 is used. The occurrence of the undamage

signal in the January 1, March 19, March 18, and July 31 acceleration records recorded during a local time of 00:00 - 01:00 is plotted in Figures 5.11 5.12 5.13, and 5.14.

Damage signals are identified using the unidentified pulses in the July 31 acceleration records. The two detected damage signals,  $T_1^D$  (blue) and  $T_2^D$  (green) are shown in Figure 5.10.  $T_1^{UD}$  and  $T_2^D$  seem to be caused by the same source and mechanism, vehicle loading at the north end of the bridge.  $T_2^D$  seems to consist of higher-frequency energy content than  $T_1^{UD}$ . On the other hand, damage signal  $T_1^D$  seems to be generated by vehicle loading at the south end of the bridge. The previously recorded data is screened for the presence of the damage signal. Again, a threshold value of 0.35 is used. The damage signal is not detected during the January 1, January 17, February 3, or March 19 acceleration records that were recorded during the same local time. The damage signals are first detected in the March 30 acceleration record, and they are detected in all subsequent records. This indicates that the dynamic response of the bridge to vehicle loading is different in the damaged and undamaged state. The occurrence of damage signal  $T_1^D$  might indicate the progression of damage, while an increase in the occurrence of the undamage signal  $T_1^{UD}$  might indicate a progression of damage.

Assuming similar traffic loads were encountered on different days at the same local time, it seems that when the bridge was in an undamaged state, a few (presumably heavy) vehicles excited a large dynamic response in the structure. When damage occurred in the bridge, a change in the physical properties of the bridge occurred that resulted in the ability of most vehicles to excite a large dynamic response in the structure, presumably due to an increase in flexibility. If the observed traveling wave is generated by the rapid loading generated as a vehicle drives onto the bridge, this would indicate that the increased flexibility occurred between the outside sensor and the end of the bridge (i.e., between the south end of the bridge and the first sensor, and between the north end of the bridge and the fourteenth sensor). Additional analysis would be needed to determine if the increased flexibility is caused by damage to the stay cables, bridge girders, or other reasons. Low-frequency strain data recorded on the cable stays could be used to assess cable damage. It would be advantageous to combine this method with a traditional vibration method, as decreases in natural frequencies

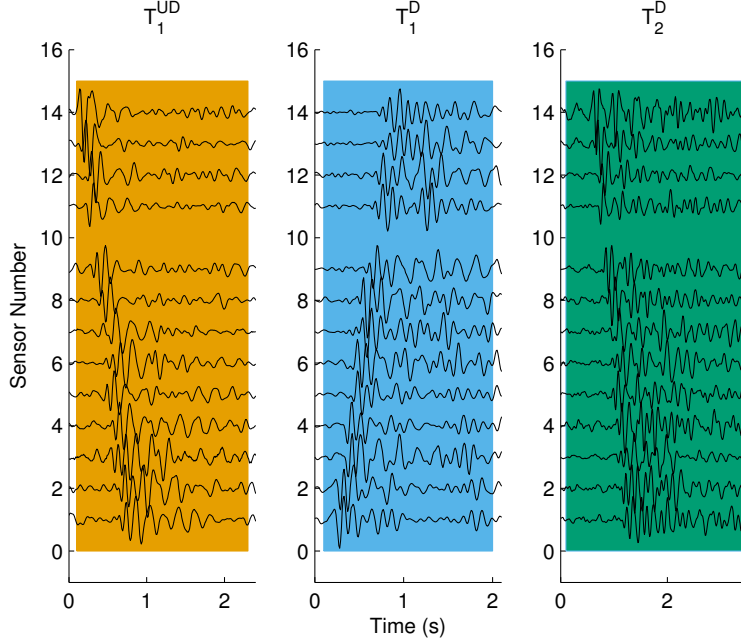


Figure 5.10: **Undamage and Damage Signals.** The undamage signal  $T_1^{UD}$  (yellow) is identified in the acceleration data recorded on January 1 between local times of 00:00-01:00. The signal originates at the north end of the bridge, and the source is most likely due to heavy vehicle loading. Two damage signals  $T_1^D$  (blue) and  $T_2^D$  (green) are identified in the acceleration data recorded on July 31 between a local time of 00:00-01:00. The signal originates at the north end of the bridge, and the source is most likely due to vehicle loading.  $T_1^{UD}$  and  $T_2^D$  seem to be caused by the same source and mechanism, though  $T_2^D$  seems to have higher frequency content. The data were high-pass filtered using a  $2^{nd}$  order Butterworth filter with a cut-off frequency of 5 Hz.

were observed. It might also be possible to stack the detected signals to obtain a high SNR, and to use an updated FEM model to perform a time-reversed reciprocal method.

### 5.3 Conclusion

The presence of high-frequency short-duration signals in the acceleration records were observed to indicate damage in two benchmark problems, the LANL nonlinear frame and the SMC damaged cable-stayed bridge. In each example, the damage signals were successfully isolated by applying a method to identify potential damage signals through feature extraction of pulses. The method effectively uses the matched filter method to detect the occurrence of repeating signals, and identify new pulses that could indicate damage.

In the LANL nonlinear frame example, the damage signal took the form of elastic waves

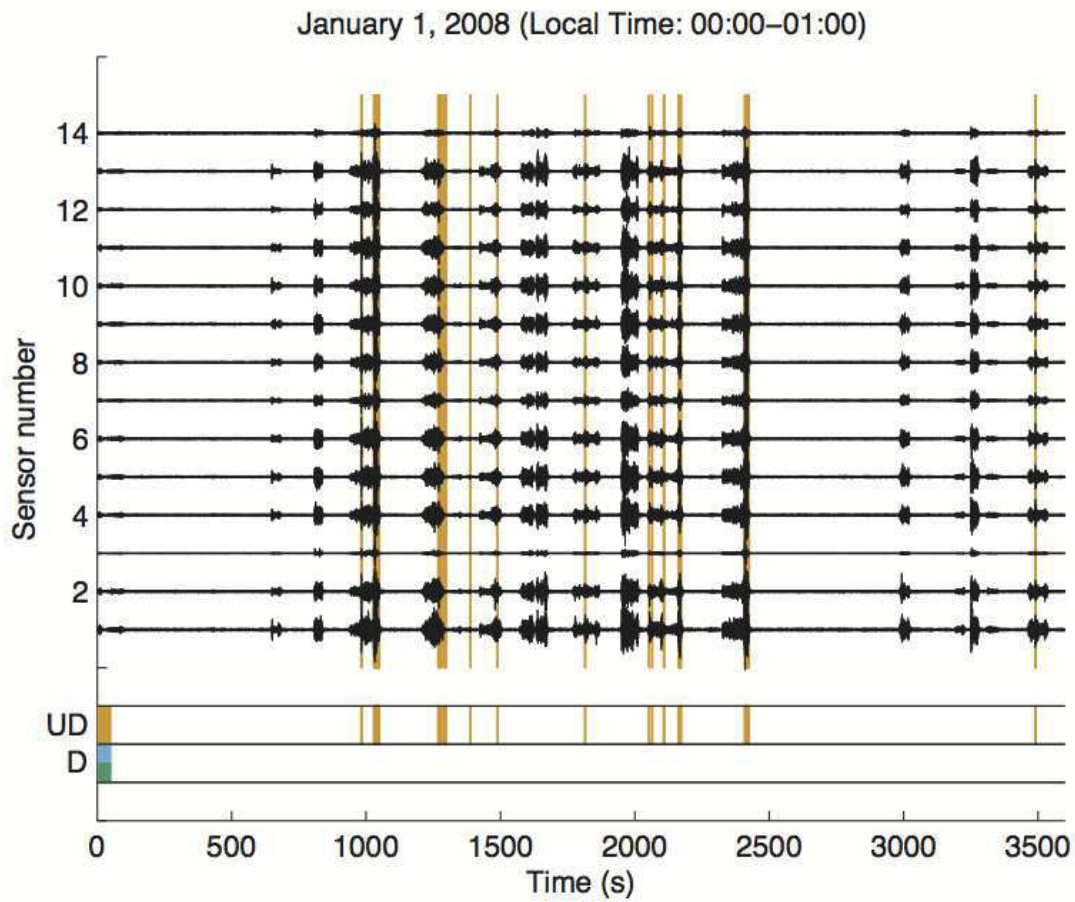


Figure 5.11: **Cable-Stayed Bridge: January 1 Acceleration Records.** The acceleration records are shown when the bridge is known to be in an undamaged state, and during light traffic conditions. The undamage signal  $T_1^{UD}$  (yellow) is identified based on pulses in the acceleration data, and a threshold value of 0.35 is used to detect the additional occurrences of the undamage signal.

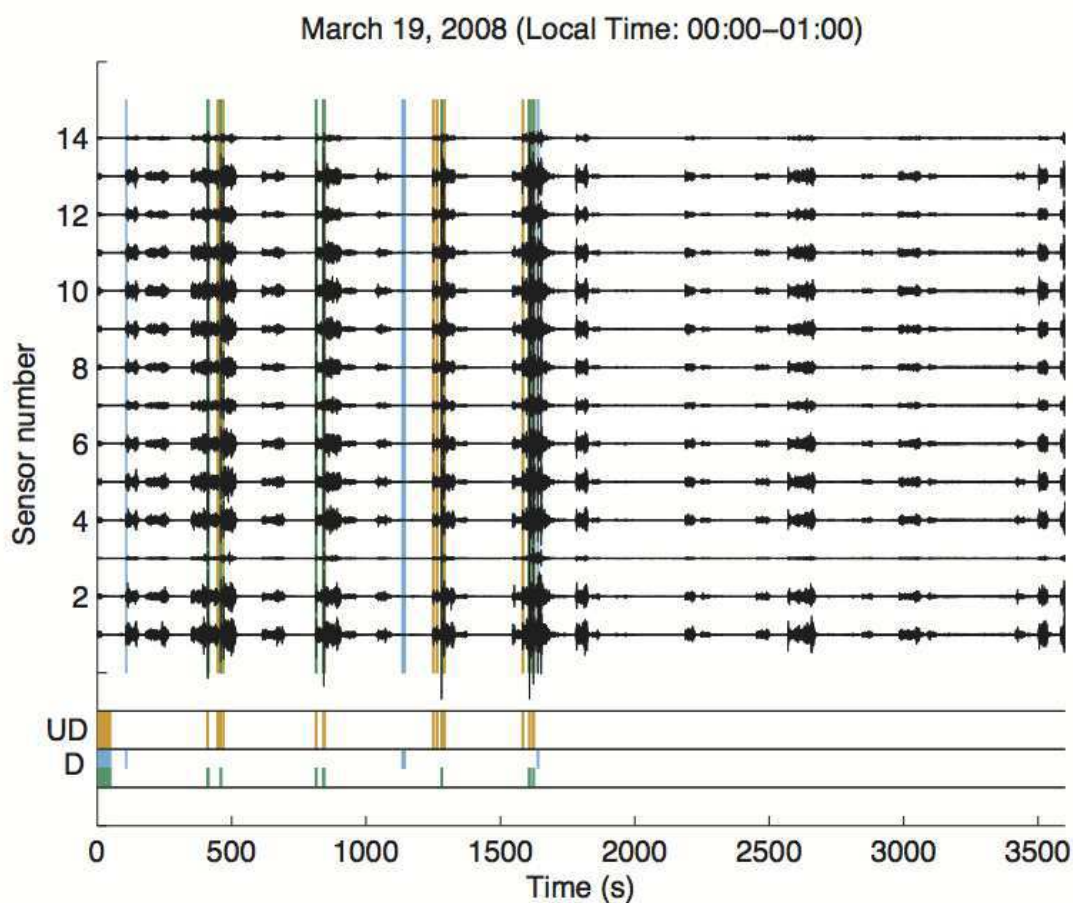


Figure 5.12: **Cable-Stayed Bridge: March 19 Acceleration Records.** The acceleration records are shown when the bridge is not known to be in an undamaged or damaged state, and during light traffic conditions. The undamage signal  $T_1^{UD}$  (yellow) is identified multiple times in the data. The first detected occurrences of damage signals  $T_1^D$  and  $T_2^D$  at this time of day are present in this data set.

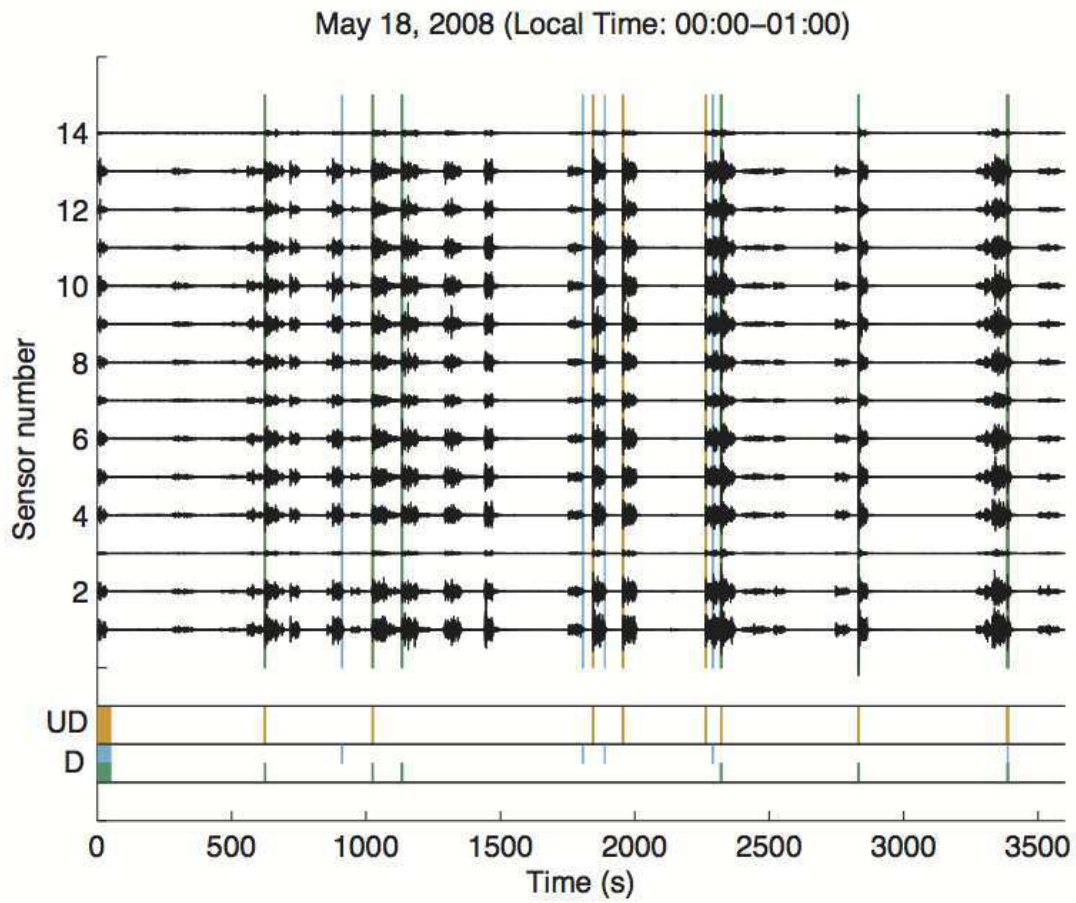


Figure 5.13: **Cable-Stayed Bridge: May 18 Acceleration Records.** The acceleration records are shown when the bridge is not known to be in an undamaged or damaged state, and during light traffic conditions. The undamage signal  $T_1^{UD}$  (yellow) and damage signals  $T_1^D$  and  $T_2^D$  are detected multiple times.

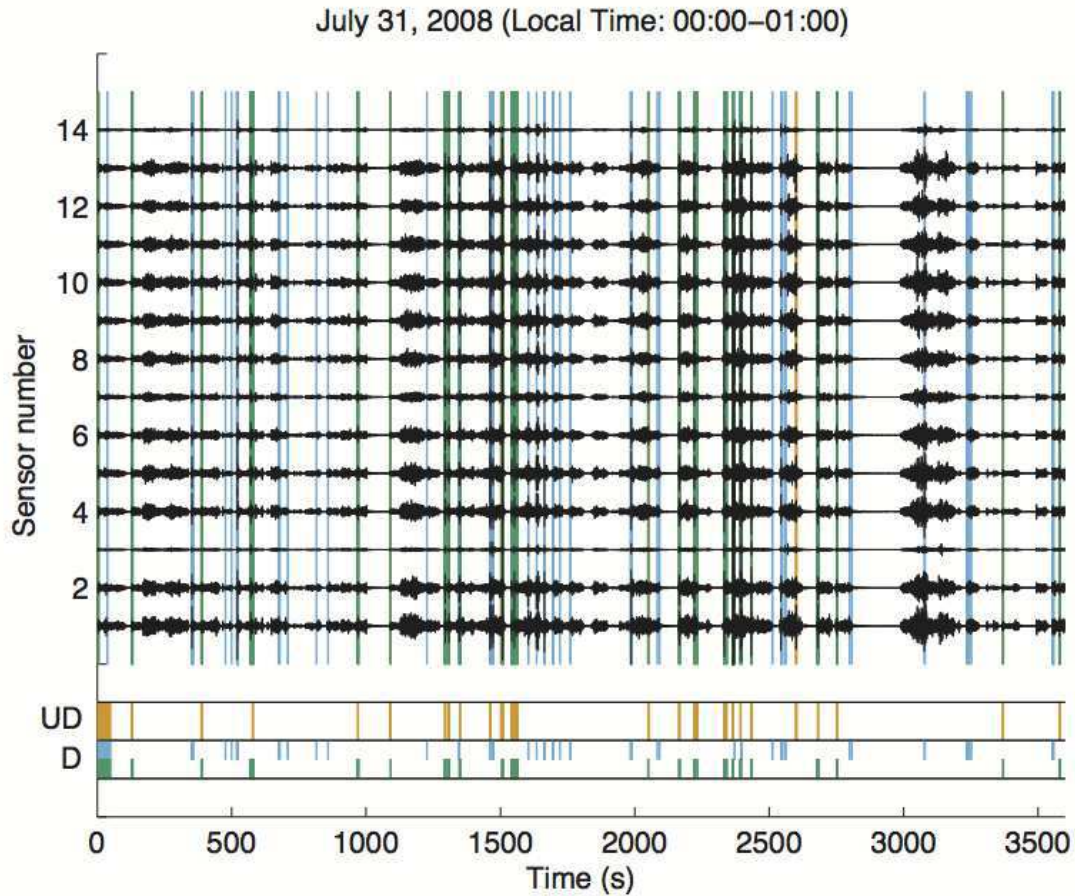


Figure 5.14: **Cable-Stayed Bridge: July 31 Acceleration Records.** The acceleration records are shown when the bridge is known to be in a damaged state, and during light traffic conditions. The undamage signal  $T_1^{UD}$  (yellow) is detected multiple times in the record. Two damage signals,  $T_1^D$  (blue) and  $T_2^D$  (green), are identified based on the unidentified pulses in the July 31 acceleration records.  $T_1^D$  seems to be generated by vehicle loading at the north end of the bridge;  $T_2^D$  seems to be generated by vehicle loading at the south end of the bridge.  $T_1^{UD}$  and  $T_2^D$  seem to be generated by the same source and mechanism, with higher-frequency content in  $T_2^D$ . The occurrence of damage signal  $T_1^D$  might indicate the progression of damage, while the change in the undamage signal  $T_1^{UD}$  might indicate a progression of damage. The data were high-pass filtered using a  $2^{nd}$  order Butterworth filter with a cut-off frequency of 5 Hz.

generated by the impact of a bumper mechanism. By using either high-pass filtering or a time-frequency representation, the damage signal could be clearly detected as high-frequency pulses in the acceleration records obtained on the two floors housing the bumper mechanism. The method was observed to be robust despite the low sampling rate, though an increase in false negatives was observed. Additional false negatives occur at high levels of damage when there was little time separation between damage signals. However, the damage signal was successfully isolated, and it was possible to localize the damage, based on the amplitudes of the damage signals, to the top two floors of the structure.

Acceleration data was obtained from a damaged cable-stayed bridge in China. An increase in high-frequency short-duration pulses is clearly observed in the acceleration records, and the occurrence of these pulses alone might be used to indicate the presence of damage. An abrupt decrease in acceleration levels that was caused by preventative measures taken to limit traffic to prevent the collapse of the bridge indicated that the pulses are primarily caused by traffic. One undamage ( $T_1^{UD}$ ) and two damage signals ( $T_1^D$  and  $T_2^D$ ) were isolated using the feature extraction method. Damage signal  $T_1^D$  appears to be generated by vehicle loading on the south end of the bridge; signals  $T_1^{UD}$  and  $T_2^D$  seem to have been generated by the same source mechanism and location, namely vehicle loading on the north end of the bridge. All acceleration data (recorded during the same time period during light traffic) was screened for the presence of the undamage and damage signals using a threshold value of 0.35. The undamage signal is detected multiple times in each dataset. The damage signals were first detected in the March 30 acceleration record, and they were also detected multiple times in all subsequent records. This is consistent with the occurrence of damage signal  $T_1^D$  indicating the progression of damage, and the change in the undamage signal  $T_1^{UD}$  indicating a progression of damage. Assuming similar traffic loads were encountered on different days at the same local time, it seems that when the bridge was in an undamaged state, a few (presumably heavy) vehicles excited a large dynamic response in the structure. When damage occurred in the bridge, a change in the physical properties of the bridge occurred that resulted in the ability of most vehicles to excite a large dynamic response in the structure, presumably due to an increase in flexibility. If the observed traveling wave is generated by

the rapid loading event that occurs as a vehicle drives onto a region of increased flexibility on the bridge, this would indicate that the damage location is located between each outside sensor and the closest end of the bridge (i.e., between the south end of the bridge and the first sensor, and between the north end of the bridge and the fourteenth sensor). Additional analysis would be needed to determine if the increased flexibility is caused by damage to the stay cables, bridge girders, or other reasons. Low-frequency strain data recorded on the cable stays could be used to assess cable damage. It would be advantageous to combine this method with a traditional vibration method, as decreases in natural frequencies were observed.

There is some art in choosing the threshold value; too high a threshold value will result in false negatives (missed detections), and too low a threshold value will result in false positives. It might be possible to determine an optimal threshold value by actively exciting the structure using a few known sources (i.e. hammer blow or a known car of a given speed) over the course of a few weeks and experimentally determining an appropriate range based on the analysis of the method using the known signals.

There is also some art in choosing the filtering threshold. It is relatively easier to do this for simple experimental models that are excited along a single axis – a cut-off frequency above the predominant modal frequencies of the structure is desired, and the number of modes to consider is approximately given by the number of floors. For full-scale structures *in situ*, different modes are excited during different environmental conditions, and numerical models typically have a larger number of modes than are excited in the real structure. Model reduction can be used to estimate the highest mode present in the real structure and hence the highest mode above which to filter. Finally, some consideration must be given to the frequency content of the damage signal. Different frequencies are expected to be emitted for different damage mechanisms (e.g. acoustic emission, mechanical impact, generation of a flexural wave).

Finally, while applying the feature detection method can successfully isolate the damage signal in the case of known damage to a structure with a baseline recording, the ability of the technique to quantitatively determine the severity of damage (i.e., loss in stiffness or

increase in flexibility), and hence to definitively determine the presence of damage, is lacking. Changes in the dynamic behavior of the structure can be identified using outlier methods, changes in damage severity can be determined qualitatively, and the damage signal can be used to determine where damage occurred and give an energy estimate, but the damage signal cannot on its own be used to determine the loss in stiffness of the structure, and hence should be combined with knowledge of the structure (e.g., a finite-element model with knowledge of potential damage locations and mechanisms), a statistical approach using data recorded on multiple damaged structures of a similar type (these data would need to be experimentally obtained), or a complementary vibration-based damage detection method.